Isomers on the $Si_2CH_4^+$ Potential Energy Surface

Jerzy Moc,† Kiet A. Nguyen, and Mark S. Gordon*

Department of Chemistry, Iowa State University, Ames, Iowa 50011

Received August 23, 1996[⊗]

The $Si_2CH_4^+$ potential energy surface has been studied theoretically using *ab initio* unrestricted Hartree−Fock, restricted open shell Hartree−Fock, and fourth-order perturbation theories. In addition to the formation of ion−molecule complexes, several rearrangements to other isomers are possible. The transition states connecting the isomers have been determined, and the minimum energy paths have been traced from isomer to isomer via the connecting transition states.

Introduction

Gas phase chemical reactions of small silicon cluster ions with different reagent molecules have made it possible to gain insight into chemical vapor deposition and etching and thus to gain a better understanding of these important processes.[1] In particular, the reactions of Si^+ with several small molecules have recently attracted considerable attention.[2] Of special interest has been the reaction of Si^+ with methylsilane (SiH_3CH_3) which has been studied by several experimental groups.[3] One of the two major products observed in this reaction at thermal energies was the $Si_2CH_4^+$ ion, indicating the relative stability of this species. In the experiment by Mayer and Lampe,[3a] who used a tandem mass spectrometer, only small amounts of $Si_2CH_4^+$ were observed, together with the predominant ionic products $SiCH_3^+$ and $SiCH_5^+$. In contrast, Mandich et al.[3b] observed only $Si_2CH_4^+$ and $SiCH_3^+$ as products in the reaction between Si^+ and SiH_3CH_3 under low pressure in the ion trap cell of a fourier transform mass spectrometer. No other ionic products were seen by these researchers[3b] at thermal energies. The most recent experimental study on the reaction of Si^+ with methylsilane was conducted by Armentrout and co-workers[3c] with kinetic energies ranging from thermal to 10 eV by using guided ion beam mass spectrometry. Ten different ionic products were observed by Armentrout[3c] with $Si_2CH_4^+$ and $SiCH_3^+$ again being the major ionic products at thermal energies.

On the theoretical side, the reaction of Si^+ with SiH_3CH_3 was investigated by Raghavachari[4a] and very recently by Nguyen et al.[4b] In the comprehensive work by the latter authors, three different mechanisms were studied in detail. Each of these mechanisms involve initial complex formation, followed by insertion of Si^+ into the Si−C, Si−H, and C−H bonds, eventually leading to the elimination of H_2 and other products. In particular, Nguyen et al.[4b] explored several H_2 elimination channels from the $Si_2CH_6^+$ intermediates yielding the $Si_2CH_4^+$ species. Most of these processes were shown to be exothermic. The computed[4b] net barriers to the H_2 elimination from $Si_2CH_6^+$ ranged from −10.2 to 14.1 kcal/mol, relative to the initial reactants. Thus, some of the H_2 elimination reactions (with no overall barriers) were predicted[4b] to occur at thermal energies. This is consistent with the experimental results of Mayer and Lampe[3a] and Mandich et al.[3b]

In the present work we report an *ab initio* theoretical study of the interaction between Si^+ and silaethylene, SiH_2CH_2, leading to the formation of the $Si_2CH_4^+$ ion which, as mentioned above, is one of the major products formed during the reaction of Si^+ with SiH_3CH_3 at thermal energies. A portion of the potential energy surface (PES) for the species $Si_2CH_4^+$ has been explored in order to determine the isomeric structures of $Si_2CH_4^+$ and the transition states (TS) connecting them, as well as the associated energetics. These theoretical data facilitate the prediction of the relevant isomerization pathways. When relevant, our results are compared with those computed earlier[4] for the $Si^+ + SiH_3CH_3$ process.

Computational Methods

Geometry optimizations of closed- and open-shell species were performed at the restricted Hartree−Fock (RHF) and unrestricted Hartree−Fock (UHF) levels of theory, respectively. For consistency with the previous calculations,[4] the 6-31G(d) basis set[5] was utilized for this purpose. It is possible that the use of UHF wavefunctions can lead to significant spin contamination, as measured (for example) by the deviation of the spin squared average value $\langle S^2 \rangle$ from the exact value of 0.75 for doublet states of radicals. To study the effects of spin contamination on the calculated $Si_2CH_4^+$ structures, geometry optimizations using restricted open-shell Hartree−Fock (ROHF) wavefunctions were also carried out. For the majority of cases, these effects were found to be negligible; thus, the UHF structures are reported and discussed at length. At the same time, the important differences between the UHF and ROHF

† Permanent address: Faculty of Chemistry, Wroclaw University, F. Joliot-Curie 14, 50-383 Wroclaw, Poland.

[⊗] Abstract published in *Advance ACS Abstracts,* November 15, 1996.

(1) Mandich, M. L.; Reents, W. D.; Kolenbrander, K. D. *Pure and Appl. Chem.* **1990**, *62*, 1653.

(2) (a) Wlodek, S.; Fox, A.; Bohme, D. K. *J. Am. Chem. Soc.* **1991**, *113*, 4461 (CH_4, C_2H_6, C_2H_4, C_2H_2, CH_2CCH_2, CH_3CCH, and C_4H_2). (b) Stewart, G. W.; Henis, J. M. S.; Gaspar, P. P. *J. Chem. Phys.* **1972**, *57*, 1990 (CH_4). (c) Boo, B. H.; Elkind, J. L.; Armentrout, P. B. *J. Am. Chem. Soc.* **1990**, *112*, 2083 (CH_4). (d) Boo, B. H.; Armentrout, P. B. *J. Am. Chem. Soc.* **1991**, *113*, 6401 (CH_3CH_3).

(3) (a) Mayer, T. M.; Lampe, F. W. *J. Phys. Chem.* **1988**, *92*, 6284. (b) Mandich, M. L.; Reents, W. D.; Bondybey, V. E. *J. Phys. Chem.* **1986**, *90*, 2315. (c) Kickel, B. L.; Fisher, E. R.; Armentrout, P. B. *J. Phys. Chem.* **1992**, *96*, 2603.

(4) (a) Raghavachari, K. *J. Phys. Chem.* **1988**, *92*, 6284. (b) Nguyen, K. A.; Gordon, M. S.; Raghavachari, K. *J. Phys. Chem.* **1994**, *98*, 6704.

(5) (a) Gordon, M. S. *Chem. Phys. Lett.* **1980**, *76*, 163. (b) Hehre, W. J.; Ditchfield, R.; Pople, J. A. *J. Chem. Phys.* **1972**, *56*, 2257.

(6) (a) Hariharan, P. C.; Pople, J. A. *Theor. Chim. Acta* **1973**, *28*, 213. (b) Francl, M. M.; Pietro, W. J.; Hehre, W. J.; Binkley, J. S.; Gordon, M. S.; DeFrees, J. D.; Pople, J. A. *J. Chem. Phys.* **1982**, *77*, 3654.

S0276-7333(96)00730-3 CCC: $12.00

predictions are reported. In addition, the unique ROHF structures (*vide infra*) are presented (a complete set of the Cartesian coordinates corresponding to the ROHF optimized geometries is given in the Supporting Information). For some species, the UHF-based quadratic configuration interaction (QCISD) procedure[7e] was also employed for geometry optimization.

All stationary points were verified to be either minima or transition states by computing (analytically) and diagonalizing the associated hessians (energy second derivative matrices) at both the UHF and ROHF levels. To verify the reactants and products connected by a particular transition state, the UHF intrinsic reaction coordinate (IRC)[10] was determined for each isomerization. That is, the steepest descent path was traced from each TS toward the respective reactant and product. Determining an IRC is important here because the majority of the transition states on this potential energy surface have no symmetry (*vide infra*), and it is not always transparent which reactant and product they connect. For selected isomerizations, especially those for which the UHF structures are appreciably spin-contaminated, the comparative intrinsic reaction coordinate using the ROHF wavefunction was calculated as well. All the minimum energy paths were determined by using the Gonzalez−Schlegel second-order method.[10f,g]

As in the previous work,[4b] the final energetics were determined by single point calculations including electron correlation through full fourth-order Møller−Plesset (MP4) perturbation theory[7a,b] (with spin projection[11] (PUMP4) for the open-shell species) and employing the larger 6-31G(d,p) basis set.[6] In a few cases, in particular for the lowest-energy $Si_2CH_4^+$ structures, the UHF-based coupled cluster (CCSD(T)) technique[7c,d] was also utilized. Also, for selected low-energy minima and transition states, the ROHF-based second-order perturbation theory, designated ROMP2 here, was employed.[14] The RHF, UHF, and correlated UMPn calculations were carried out by means of the GAUSSIAN92 program,[8] whereas the ROHF and ROMP2 computations were accomplished with the GAMESS code.[9]

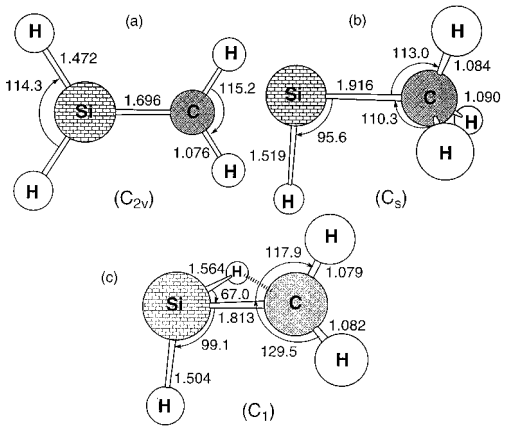

Figure 1. Optimized structures of (a) silaethylene (SiH_2-CH_2), (b) methylsilylene ($SiHCH_3$), and (c) transition state (TS) for the 1,2-hydrogen shift from silaethylene to methylsilylene. The corresponding MP4/6-31G(d,p) energies (in hartrees) are the following: for silaethylene, −329.32133; for methysilylene, −329.32150; for TS connecting silaethylene with methylsilylene, −329.25856.

As is typical for ion−molecule reactions, the potential energy surface for the reaction of Si^+ with silene is complex. Initial formation of ion−molecule complexes may be followed by various insertions into adjacent bonds, as well as other rearrangements. A key question with regard to each rearrangement is whether the associated barrier height is higher or lower in energy than the separated reactants, since this determines the accessibility of the various minima at low temperatures. Since final energetics are determined at a higher level of theory than that used to determine the geometries of minima and transition states, it is possible that apparent stationary points on the self-consistent field surface will disappear when correlation corrections are added. These complications are discussed in the next section as they occur.

Results and Discussion

The optimized structures of the two most stable isomers of $SiCH_4$, i.e., SiH_2CH_2 and $SiHCH_3$, along with the transition state connecting them are depicted in Figure 1. Figure 2 shows the UHF geometries corresponding to the minima on the $Si_2CH_4^+$ energy surface, while the transition states connecting these minima are displayed in Figure 3. In turn, the total energies, zero point vibrational energies (ZPE), and $\langle S^2 \rangle$ values are compiled in Table 1, and the various relative energies are compared in Tables 2 and 3. Finally, Figure 4 illustrates the composite PUMP4/6-31G(d,p) potential energy diagram for $Si_2CH_4^+$, whereas the unique transition states obtained at the ROHF level are shown in Figure 5.

Reactants. Closed-shell singlet silaethylene, SiH_2-CH_2 (Figure 1a), and methylsilylene, $SiHCH_3$ (Figure 1b), have been the subject of considerable theoretical interest focused on comparing their thermodynamic stabilities and estimating the magnitude of the barrier to the 1,2-hydrogen shift connecting them.[12,13] *Ab initio* calculations conclude that singlet silaethylene and singlet methylsilylene lie close in energy; the best prediction of the respective energy difference is about 4 kcal/mol, with the silaethylene predicted to be the more stable isomer.[12b] There is a substantial energy

(7) (a) Krishnan, R.; Frisch, M. J.; Pople, J. A. *J. Chem. Phys.* **1980**, *72*, 4244. (b) Bartlett, R. J.; Sekino, H.; Purvis, G. D. *Chem. Phys. Lett.* **1983**, *98*, 66. (c) Scheiner, A. C.; Scuseria, G. E.; Rice, J. E.; Lee, T. J.; Schaefer, H. F. *J. Chem. Phys.* **1987**, *87*, 5361. (d) Bartlett, R. D. *J. Phys. Chem.* **1989**, *93*, 1697. (e) Pople, J. A.; Head-Gordon, M.; Raghavachari, K. *J. Chem. Phys.* **1987**, *87*, 5968.

(8) GAUSSIAN92: Frisch, M. J.; Trucks, G. W.; Head-Gordon, M.; Gill, P. M. W.; Wong, M. W.; Foresman, J. B.; Johnson, B. G.; Schlegel, H. B.; Robb, M. A.; Replogle, E. S.; Gomperts, R.; Andres, J. L.; Raghavachari, K.; Binkley, J. S.; Gonzalez, C.; Martin, R. L.; Fox, D. J.; DeFrees, D. J.; Baker, J.; Stewart, J. J. P.; Pople, J. A. Gaussian, Inc., Pittsburgh, PA, 1992.

(9) GAMESS (General Atomic and Molecular Electronic Structure System): Schmidt, M. W.; Baldridge, K. K.; Boatz, J. A.; Elbert, S. T.; Gordon, M. S.; Jensen, J. H.; Koseki, S.; Matsunaga, N.; Nguyen, K. A.; Su, S.; Windus, T. L.; Dupuis, M.; Montgomery, J. A. Jr., *J. Comput. Chem.* **1993**, *14*, 1347.

(10) (a) Fukui, K. *Acc. Chem. Res.* **1981**, *14*, 363. (b) Ishida, K.; Morokuma, K.; Komornicki, A. *J. Chem. Phys.* **1977**, *66*, 2153. (c) Schmidt, M. W.; Gordon, M. S.; Dupuis, M. *J. Am. Chem. Soc.* **1985**, *107*, 2585. (d) Garrett, B. C.; Redmon, M. J.; Steckler, R.; Truhlar, D. G.; Baldridge, K. K.; Bartol, D.; Schmidt, M. W.; Gordon, M. S. *J. Chem. Phys.* **1988**, *92*, 1476. (e) Baldridge, K. K.; Gordon, M. S.; Steckler, R.; Truhlar, D. G. *J. Chem. Phys.* **1989**, *93*, 5107. (f) Gonzalez, C.; Schlegel, H. B. *J. Chem. Phys.* **1989**, *90*, 2154. (g) Gonzalez, C.; Schlegel, H. B. *J. Phys. Chem.* **1990**, *94*, 5523.

(11) Schlegel, H. B. *J. Chem. Phys.* **1986**, *84*, 4530.

(12) (a) Allendorf, M.; Melius, C. *J. Phys. Chem.* **1992**, *96*, 428. (b) Grev, R. S.; Scuseria, G. E.; Scheiner, A. C.; Schaefer, H. F., III; Gordon, M. S. *J. Am. Chem. Soc.* **1988**, *110*, 7337. (c) Luke, B. T.; Pople, J. A.; Krogh-Jesperson, M. B.; Apeloig, Y.; Karmi, M.; Chandrasekhar, J.; Schleyer, P.v.R. *J. Am. Chem. Soc.* **1986**, *108*, 270. (d) Luke, B. T.; Pople, J. A.; Krogh-Jesperson, M. B.; Apeloig, Y.; Chandrasekhar, J.; Schleyer, P.v.R. *J. Am. Chem. Soc.* **1985**, *107*, 537. (e) Gordon, M. S.; Truong, T. N. *Chem. Phys. Lett.* **1987**, *142*, 110. (f) Goddard, J. D.; Yoshioka, Y.; Schaefer, H. F., III *J. Am. Chem. Soc.* **1980**, *102*, 7644. (g) Yoshioka, Y.; Schaefer, H. F., III *J. Am. Chem. Soc.* **1981**, *103*, 7366. (h) Kohler, H. J.; Lischka, H. *J. Am. Chem. Soc.* **1982**, *104*, 5884.

(13) Gordon, M. S.; Francisco, J. S.; Schlegel, H. B. *Advances in Silicon Chemistry;* JAI Press: London, 1993; Vol. 2, pp 137−185 and references cited therein. For a list of *ab initio* papers on the silaethylene and methylsilylene prior to 1980, see ref 12f.

(14) For a comparison of the various open-shell perturbation theories based on a restricted Hartree−Fock reference wavefunction, see: Lee, T. J.; Rendell, A. P.; Dyall, K. G.; Jayatilaka, D. *J. Chem. Phys.* **1994**, *100*, 7400.

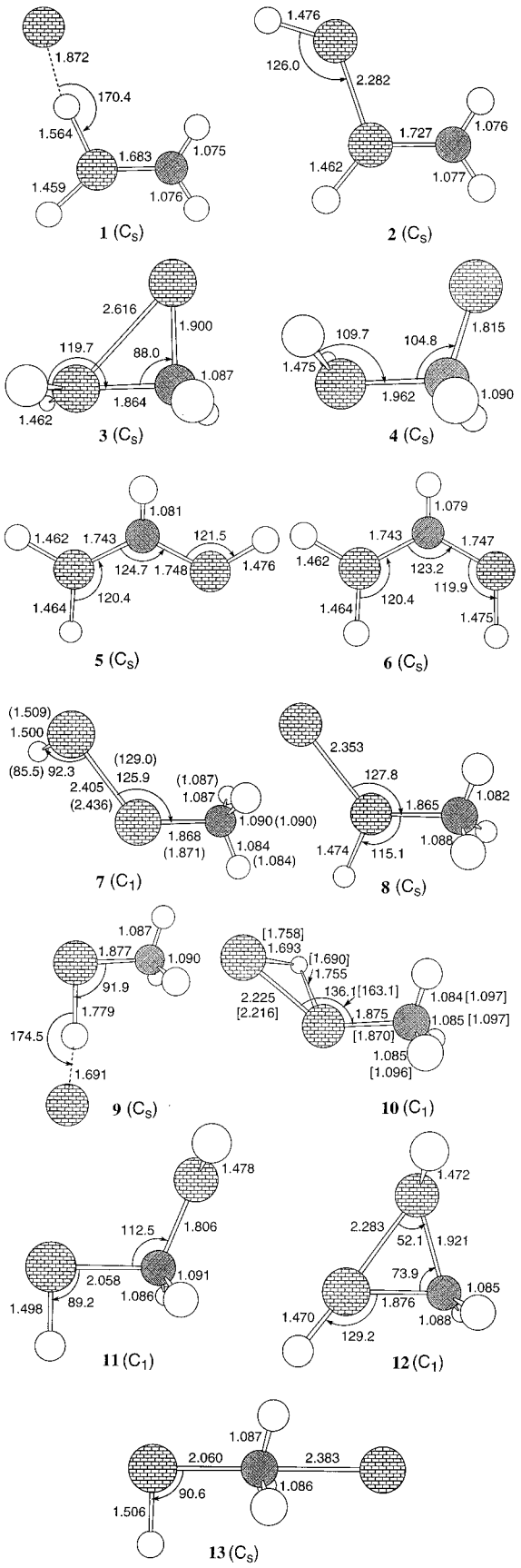

Figure 2. Minima found on the potential surface for the reaction $Si^+ + SiH_2CH_2$. Hydrogen atoms are represented as open circles, whereas silicon and carbon atoms are shown as shaded circles (cf. Figure 1). Results are from the UHF calculations unless specified otherwise. Values in parentheses for **7** are from the ROHF calculation, whereas those in brackets for **10** were obtained at the UQCISD level.

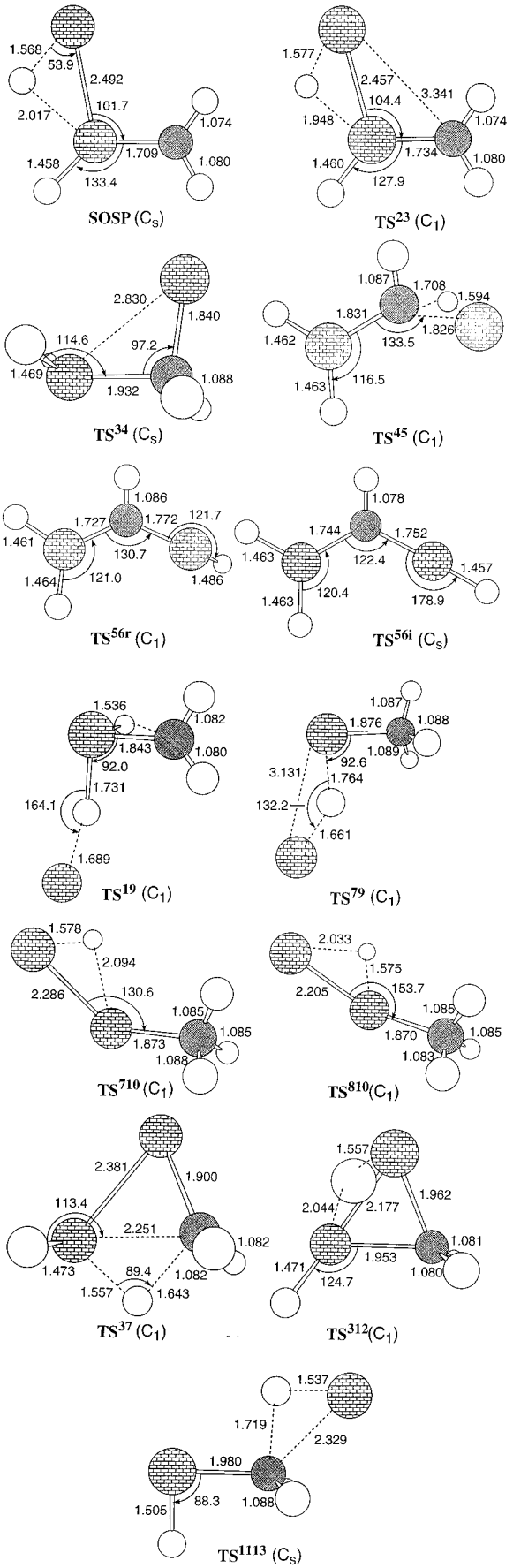

Figure 3. Transition states connecting minima shown in Figure 2. Hydrogen atoms are represented as open circles, whereas silicon and carbon atoms are shown as shaded circles (cf. Figure 1). Results are from the UHF calculations, and SOSP stands for the second-order saddle point.

Table 1. UMP4 and PUMP4 Total Energies (in Hartrees) Computed with the 6-31G(d,p) Basis Set[a]

structure	state	$\langle S^2 \rangle$	UMP4	PUMP4	ZPE[b]
$Si^+(^2P) + SiH_2CH_2$			−617.92440	−617.92503	27.0
$Si^+(^2P) + SiHCH_3$			−617.92457	−617.92520	28.1
1 (C_s)	$^2A''$	0.76	−617.95245	−617.95344	26.5
2 (C_s)	$^2A'$	0.76	−617.98838	−617.98909	27.3
3 (C_s)	$^2A'$	0.77	−618.03313	−618.03438	27.7
4 (C_s)	$^2A'$	0.80	−618.02441	−618.02634	27.4
5 (C_s)	$^2A'$	0.77	−618.01466	−618.01560	26.5
6 (C_s)	$^2A'$	0.77	−618.01583	−618.01669	26.7
7 (C_1)	^2A	1.08	−618.01339	−618.02016	28.8
8 (C_s)	$^2A''$	0.76	−618.03808	−618.03869	30.0
9 (C_s)	$^2A''$	0.76	−617.99058	−617.99150	27.8
10 (C_1)	^2A	0.98	−618.02623	−618.03209	28.9
11 (C_1)	^2A	0.76	−617.98092	−617.98131	26.6
12 (C_1)	^2A	0.82	−617.99182	−617.99402	27.3
13 (C_1)	$^2A''$	0.76	−617.96546	−617.96639	28.2
SOSP (C_s)	$^2A'$	0.77	−617.94837	−617.94973	24.5
TS[23] (C_1)	^2A	0.86	−617.95112	−617.95477	25.2
TS[34] (C_s)	$^2A'$	0.79	−618.02903	−618.03107	26.9
TS[45] (C_1)	^2A	0.82	−617.97202	−617.97464	24.2
TS[56r] (C_1)	^2A	0.77	−617.99425	−617.99556	25.3
TS[56i] (C_s)	$^2A'$	0.79	−617.97136	−617.97368	25.6
TS[37] (C_1)	^2A	0.84	−617.97388	−617.97715	27.0
TS[710] (C_1)	^2A	0.98	−618.01998	−618.02598	28.2
TS[810] (C_1)	^2A	0.88	−618.02674	−618.03056	28.6
TS[78] (C_1)[c]	^2A	0.96	−618.02202	−618.02766	28.1[d]
TS[19] (C_1)	^2A	0.77	−617.91861	−617.91996	24.8
TS[79] (C_1)	^2A	0.97	−617.98693	−617.99246	27.9
TS[89] (C_s)[c]	$^2A''$	0.77	−617.99241	−617.99362	27.9[d]
TS[312] (C_1)	^2A	0.81	−617.98496	−617.98799	26.7
TS[1113] (C_s)	$^2A'$	0.80	−617.91266	−617.91524	24.1

[a] Only the valence electrons are included in the correlation calculations. The UCCSD(T)/6-31G(d,p) total energies (in hartrees, at the UHF/6-31G(d) geometries) obtained for **1** (C_s), **TS[23]** (C_1), **SOSP** (C_s), **3** (C_s), **8** (C_s), and **10** (C_1) are −617.95713, −617.95992, −617.95333, −618.03752, −618.04284, and −618.03639, respectively. [b] Zero-point energies (in kcal/mol) are from the UHF/6-31G(d) calculation unless specified otherwise.[c] At the ROHF/6-31G(d) structure (see text). [d] The ROHF/6-31G(d) value.

Table 2. PUMP4/6-31G(d,p) Energies Relative to the Si^+ (^2P) + SiH_2CH_2 Reactants (in kcal/mol)[a]

structure	state	energy		
Si^+ (^2P) + SiH_2CH_2		0.0	(0.0)	[0.0]
1 (C_s)	$^2A''$	−17.8	(−18.3)	
2 (C_s)	$^2A'$	−40.2	(−39.9)	
3 (C_s)	$^2A'$	−68.6	(−67.9)	
4 (C_s)	$^2A'$	−63.6	(−63.2)	
5 (C_s)	$^2A'$	−56.8	(−57.3)	
6 (C_s)	$^2A'$	−57.5	(−57.8)	
7 (C_1)	^2A	−59.7	(−57.9)	[−57.8]
8 (C_s)	$^2A''$	−71.3	(−68.3)	[−71.8]
9 (C_s)	$^2A''$	−41.7	(−40.9)	[−39.9]
10 (C_1)	^2A	−67.2	(−65.3)	[−65.8]
11 (C_1)	^2A	−35.3	(−35.7)	
12 (C_1)	^2A	−43.3	(−43.0)	
13 (C_s)	$^2A''$	−26.0	(−24.8)	
SOSP (C_s)	$^2A'$	−15.5	(−18.0)	
TS[23] (C_1)	^2A	−18.7	(−20.5)	
TS[34] (C_s)	$^2A'$	−66.5	(−66.6)	
TS[45] (C_1)	^2A	−31.1	(−33.9)	
TS[56r] (C_1)	^2A	−44.3	(−46.0)	
TS[56i] (C_s)	$^2A'$	−30.5	(−31.9)	
TS[37] (C_1)	^2A	−32.7	(−32.7)	
TS[710] (C_1)	^2A	−63.3	(−62.1)	[−61.1]
TS[810] (C_1)	^2A	−66.2	(−64.6)	[−66.6]
TS[78] (C_1)[b]	^2A	−64.4	(−63.3)	[−62.4]
TS[19] (C_1)	^2A	3.2	(1.0)	
TS[79] (C_1)	^2A	−42.3	(−41.4)	[−40.5]
TS[89] (C_s)[b]	$^2A''$	−43.0	(−42.1)	[−41.1]
TS[312] (C_1)	^2A	−39.5	(−39.8)	
TS[1113] (C_s)	$^2A'$	6.1	(3.2)	

[a] Numbers in parentheses include the zero-point energy correction (cf. Table 1). Values in brackets are from the ROMP2/6-31G(d,p) calculation assuming the UHF/6-31G(d) geometries unless specified otherwise. [b] At the ROHF/6-31G(d) structure.

barrier to the 1,2-hydrogen shift from silaethylene to methylsilylene, *ca.* 40 kcal/mol.[12f−h] Our RHF/6-31G(d) optimized structures of silaethylene (Figure 1a), methysilylene (Figure 1b), and the 1,2-hydrogen shift transition state (Figure 1c) are in good agreement with those computed earlier at comparable levels of theory.[12] In accordance with the previous studies, our calculations reveal that the two isomers are very close in terms of thermodynamic stability, with an energy separation of only 1.0 kcal/mol at the ZPE-corrected MP4/6-31G(d,p) level, with the silaethylene, SiH_2CH_2, found to be the more stable isomer. The MP4 barrier height for the silaethylene rearrangement of 39.4 kcal/mol compares favorably with the *ab initio* predictions noted above.[12f−h] Thus, the results of the calculations reported in this section lend credence to the theoretical model employed in the paper. Si^+ has a ^2P ground state, and we have explored here only the doublet PES for $Si_2CH_4^+$. The energetics quoted in the remainder of the paper are at the ZPE-corrected PUMP4/6-31G(d,p) level of theory, unless noted otherwise.

Complexes. A plausible structure for the interaction between Si^+ and silaethylene, SiH_2CH_2 is the ion−molecule complex **1** (Figure 2). This species arises from the interaction of Si^+ with one of the Si−H bonds in SiH_2CH_2 and lies 18 kcal/mol below $Si^+ + SiH_2CH_2$. The salient features of **1**, which has a planar C_s structure, are the stretching of the involved Si−H bond relative to that in isolated SiH_2CH_2 and the nearly linear Si−H···Si arrangement. As noted elsewhere,[4a] the polarizable nature of the Si−H bond, the sign of the bond dipole, and the inclination of H toward bridged bonding contribute to the strength of complexes of this type. The binding energy of **1** (18 kcal/mol), although quite large, is smaller than that in the complex formed between Si^+ and one of the Si−H bonds in methylsilane, SiH_3CH_3. The latter complex is more strongly bound, by about 10 kcal/mol at similar levels of theory.[4] This is consistent with the smaller stretching of the involved Si−H bond and the longer H···Si distance in **1** as compared to those in the methylsilane analogue.[4] Also, no doubly bridged complex is formed between Si^+ and two SiH_2 hydrogens, whereas such a bifurcated complex is found for the silyl group of methylsilane.[4b] Indeed, the planar C_{2v} doubly bridged complex between Si^+ and the two hydrogens on the silicon end of SiH_2CH_2 has two imaginary frequencies, thus it does not correspond to a structurally stable species. The lack of a stable doubly-bridged complex in the case of SiH_2CH_2 is probably due to the larger HSiH angle in this compound, compared with methylsilane.

Following the previous study on the methylsilane reaction,[4b] we also looked for a stable complex in which Si^+ was directly attached to the carbon atom of SiH_2-CH_2. Our computed planar C_{2v} structure with the C−Si and H···Si distances of 2.384 and 2.107 Å, respectively, could also be viewed as a doubly bridged complex between Si^+ and two CH_2 hydrogens. This structure, however, is a saddle point for a degenerate **3** ↔ **3** rearrangement as verified by tracing the IRC (see below for a detailed discussion of structure **3**). No stationary point corresponding to a complex between Si^+ and one C−H bond in SiH_2CH_2 was found.

On the basis of the similar thermodynamic stabilities of the SiH_2CH_2 and $SiHCH_3$ isomers (discussed above) and the relatively long Si−H bond in the latter structure (Figure 1), one can expect formation of a stable complex

Table 3. Relative Energies of the $Si_2CH_4^+$ Isomers and Energy Barriers for the Isomerization Reactions[a]

isomer	relative energy	reaction[b]	energy barrier	reaction[c]	energy barrier
1 (C_s)	53.5 (50.0)	**1** (C_s) → **2** (C_s)	d	**2** (C_s) → **1** (C_s)	d
2 (C_s)	31.1 (28.4)	**2** (C_s) → **3** (C_s)	21.5 (19.4)	**3** (C_s) → **2** (C_s)	50.0 (47.5)
3 (C_s)	2.7 (0.4)	**3** (C_s) → **4** (C_s)	2.1 (1.3)	**4** (C_s) → **3** (C_s)	−3.0 (−3.5)
4 (C_s)	7.7 (5.1)	**4** (C_s) → **5** (C_s)	32.4 (29.2)	**5** (C_s) → **4** (C_s)	25.7 (23.4)
5 (C_s)	14.5 (11.0)	**5** (C_s) → **6** (C_s) rot	12.6 (11.4)	**6** (C_s) → **5** (C_s) rot	13.3 (11.9)
6 (C_s)	13.8 (10.5)	**5** (C_s) → **6** (C_s) inv	26.3 (25.4)	**6** (C_s) → **5** (C_s) inv	27.0 (25.9)
7 (C_1)	11.6 (10.4)	**3** (C_s) → **7** (C_1)	35.9 (35.2)	**7** (C_1) → **3** (C_s)	27.0 (25.2)
10 (C_1)	4.1 (3.0)	**7** (C_1) → **10** (C_1)	−3.7 (−4.3)	**10** (C_1) → **7** (C_1)	3.8 (3.1)
8 (C_s)	0.0 (0.0)	**10** (C_1) → **8** (C_s)	1.0 (0.7)	**8** (C_s) → **10** (C_1)	5.1 (3.7)
		7 (C_1) → **8** (C_s)[e]	−4.7 (−5.4)	**8** (C_s) → **7** (C_1)[e]	6.9 (5.0)
9 (C_s)	29.6 (27.4)	**1** (C_s) → **9** (C_s)	21.0 (19.3)	**9** (C_s) → **1** (C_s)	44.9 (41.9)
11 (C_1)	36.0 (32.6)	**9** (C_s) → **7** (C_1)	−0.6 (−0.5)	**7** (C_1) → **9** (C_s)	17.4 (16.5)
		9 (C_s) → **8** (C_s)[f]	−1.3 (−1.2)	**8** (C_s) → **9** (C_s)[f]	28.3 (26.2)
12 (C_1)	28.0 (25.3)	**3** (C_s) → **12** (C_1)	29.1 (28.1)	**12** (C_1) → **3** (C_s)	3.8 (3.2)
13 (C_s)	45.4 (43.6)	**11** (C_1) → **13** (C_s)	41.5 (39.0)	**13** (C_s) → **11** (C_1)	32.1 (28.0)

[a] All values (in kcal/mol) computed at the PUMP4/6-31G(d,p) level; numbers in parentheses include the zero-point energy correction (cf. Table 1). "rot" and "inv" indicate the rotation and inversion, respectively. [b] Forwards. [c] Backwards. [d] The respective TS not found (see text). [e] Via the ROHF TS^{78} (C_1) (cf. Figure 5). [f] Via the ROHF TS^{89} (C_s) (cf. Figure 5).

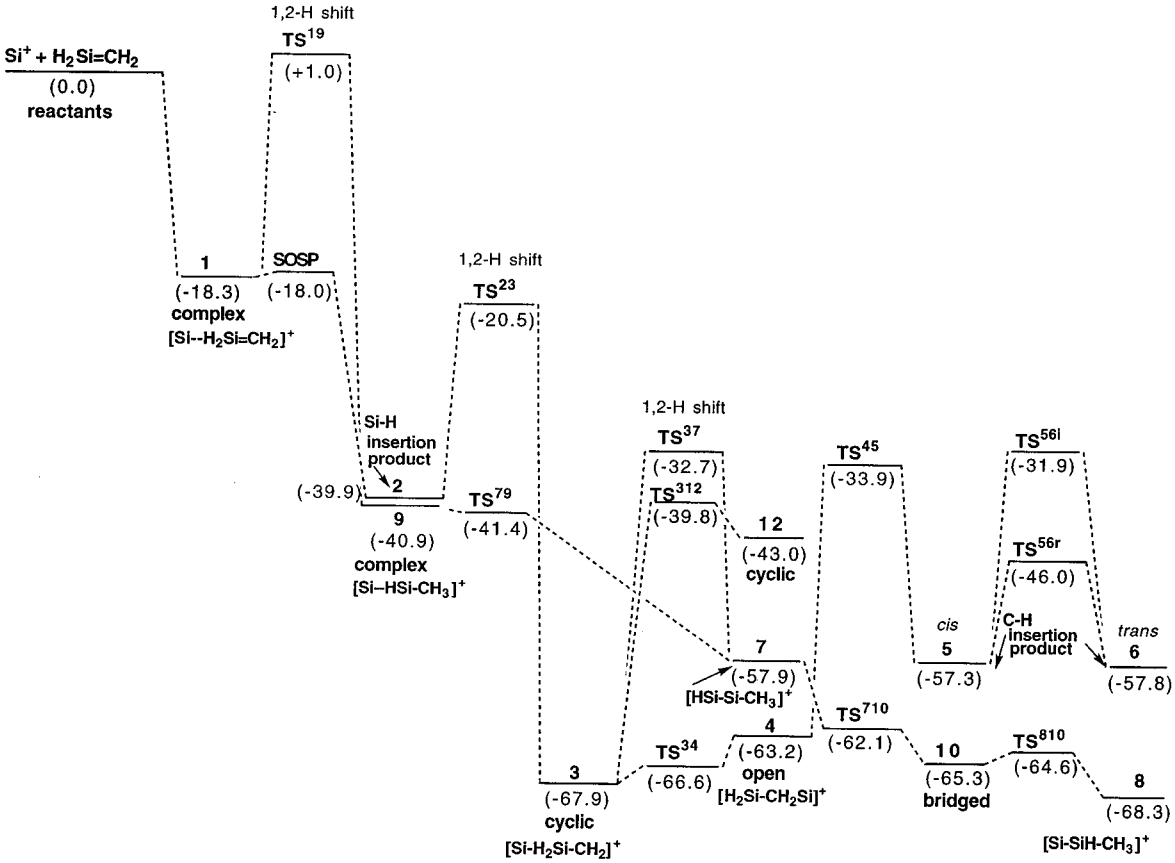

Figure 4. PUMP4/6-31G(d,p)//UHF/6-31G(d) potential energy diagram for $Si_2CH_4^+$ with zero-point vibrational energy included. All energies are in kcal/mol.

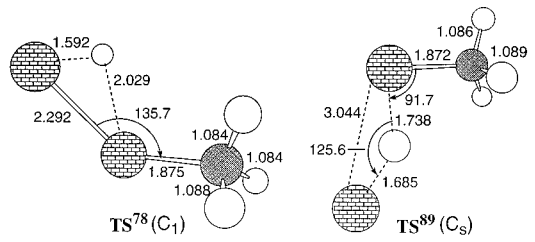

Figure 5. Unique transition states obtained at the ROHF level. Hydrogen atoms are represented as open circles, whereas silicon and carbon atoms are shown as shaded circles (cf. Figure 1).

between Si^+ and $SiHCH_3$ involving this bond. Indeed, such a complex with C_s symmetry was found and is denoted **9** in Figure 2. Complex **9** lies 41 kcal/mol below $Si^+ + SiH_2CH_2$ (Table 2 and Figure 4) and is predicted to be over 20 kcal/mol more stable than **1**. The remarkable strength of **9** is reflected in both the large (0.26 Å) stretching of its Si−H bond relative to that in isolated $SiHCH_3$ and the much shorter interacting H···Si distance as compared to **1** (1.691 vs 1.872 Å). Note that the bridging H in **9** is actually closer to the attached silicon than to its original partner (Figure 2). The Mulliken charge distribution in **9** reveals that the bridging H is very negative (−0.37e) and the attached silicon (+0.63e) is less positively charged than the other silicon (+0.82e). This is consistent with the shorter (less ionic) H-Si bond involving the terminal Si in **9**. The other prominent features of **9** are the C−Si−H bond angle of *ca.* 90° and the nearly linear Si−H···Si arrangement, as in **1**.

A transition state connecting complexes **1** and **9** is shown (**TS[19]**) in Figure 3. This 1,2-hydrogen shift TS has no symmetry and lies slightly above $Si^+ + SiH_2CH_2$ (1.0 kcal/mol at the ZPE-corrected PUMP4 level of theory, Table 2 and Figure 4). Some structural resemblance between **TS[19]** and the transition state for the 1,2-hydrogen shift from silaethylene to methylsilylene can be seen (cf. Figures 1c and 3). Walking down the minimum energy path from **TS[19]** leads to **9** and **1** for the forward and reverse directions, respectively.

Our subsequent search for a complex having Si^+ directly attached to the carbon atom of methylsilylene ($SiHCH_3$) resulted in the stable C_s species **13**. Formation of **13**, due to the interaction of Si^+ on the $-CH_3$ side of methylsilylene, parallels formation of the analogous structure in the reaction of Si^+ with methylsilane.[4b] Complex **13** has an even shorter Si−C interaction distance (2.383 Å) than that in the methylsilane analogue, by nearly 0.1 Å. In fact, **13** is more stable than **1** by 6.5 kcal/mol, lying *ca.* 25 kcal/mol below $Si^+ + SiH_2CH_2$. Complex **9** is the most thermodynamically stable of the three complexes found in the present work.

Insertion and Isomerization Reactions. Starting from the $[Si\cdots H_2Si{=}CH_2]^+$ complex **1**, other possible rearrangements include insertion of Si^+ into an attached Si−H bond or a 1,2-shift of Si^+ to the carbon. The insertion of Si^+ into an Si−H bond yields $[HSi{-}SiH{-}CH_2]^+$ (**2**), which lies 40 kcal/mol below $Si^+ + SiH_2CH_2$. Thus, structure **2** is essentially isoenergetic with the $[Si\cdots HSi{-}CH_3]^+$ complex **9** discussed above. The Si−H insertion product **2** has a planar C_s structure with a Si−Si−H bond angle of 126° (Figure 2). This angle is very similar to the corresponding value found in the intermediate formed by Si^+ insertion into an Si−H bond of SiH_3CH_3.[4] Generation of the minimum energy path connecting **1** and **2** within C_s symmetry, followed by refinement of the highest energy structure on this path, yields a second-order saddle point (two imaginary frequencies), denoted **SOSP** in Figure 3. **SOSP** is only 0.3 kcal/mol above $[Si\cdots H_2Si{=}CH_2]^+$ (**1**, Table 2 and Figure 4). At the higher UCCSD(T)/6-31G(d,p) level of theory, **SOSP** is 0.4 kcal/mol above **1** (with ZPE included). When the symmetry constraint in **SOSP** is relaxed, the geometry optimizes to **TS[23]**, i.e., the transition state connecting minima **2** and **3** (see below for a detailed discussion of **3** and **TS[23]**). **TS[23]** lies 2.2 and 3.0 kcal/mol below **1** at the ZPE-corrected PUMP4 and UCCSD(T)/6-31G(d,p) levels, respectively. We conclude from these results that the **1** → **2** insertion involves a second-order saddle point which is 18 kcal/mol below the initial reactants and that this process is therefore accessible at thermal energies.

Starting from **1**, insertions of Si^+ into the C−H and Si−C bonds of SiH_2CH_2 are also conceivable. Two C_{2v} structures corresponding to insertion into the Si−C bond of SiH_2CH_2 (planar and twisted) were examined, but neither structure is a minimum on the potential energy surface. These structures have two or more imaginary frequencies. However, there is a low-energy pathway leading to the C−H insertion product, as will be discussed below.

The Si−H insertion product $[HSi{-}SiH{-}CH_2]^+$ (**2**) can isomerize further. A 1,2-hydrogen migration from the terminal Si leads to the cyclic isomer $[Si{-}H_2Si{-}CH_2]^+$ (**3**) mentioned above. The energy requirement to traverse from **2** to **3** via a 1,2-hydrogen migration transition state, denoted **TS[23]** (Figure 3), is 19.5 kcal/mol. Despite this large barrier, **TS[23]** is 20.5 kcal/mol below $Si^+ + SiH_2CH_2$; the **2** → **3** isomerization is accessible at thermal energies. **TS[23]** is an "early" transition state, based on the forming Si−C and Si−H bond distances in **3** as well as the relatively small distortion of **TS[23]** from planarity. The cyclic C_s product **3** is predicted to be one of the two lowest energy isomers of $Si_2CH_4^+$ (*vide infra*), lying 68 kcal/mol below $Si^+ + SiH_2CH_2$ (Table 2 and Figure 4). The Si−C−Si bond angle in **3** is nearly 90°, and its two Si−C distances of 1.864 and 1.900 Å as well as the Si−Si distance of 2.616 Å are close to those found in the analogous cyclic isomer of $Si_2CH_6^+$.[4b]

It appears that the cyclic isomer $[Si{-}H_2Si{-}CH_2]^+$ (**3**) can rearrange easily to the open form $[H_2Si{-}CH_2Si]^+$ (**4**), in which the weak Si−Si bond in **3** is completely broken (with a Si···Si distance of 3.0 Å) and one of the Si−C distances is significantly lengthened, by ∼0.1 Å relative to that in **3**. Structure **4** is predicted to lie 63.2 kcal/mol below $Si^+ + SiH_2CH_2$. The transition state connecting **3** with **4** (**TS[34]** in Figure 3) is predicted to be 66.6 kcal/mol below $Si^+ + SiH_2CH_2$. Since **TS[34]** is therefore 3.5 kcal/mol *below* product **4** when correlation corrections are included in the energy calculation (Table 3 and Figure 4), **4** may not be a true minimum at higher levels of theory. In fact, **4** reverts to **3** during the UMP2/6-31G(d) optimization.

Starting from the open isomer $[H_2Si{-}CH_2Si]^+$ (**4**), Si^+ may insert into a C−H bond to produce $[H_2Si{-}CH{-}SiH]^+$ (**5**). This isomer has a planar C_s structure with a *cis* conformation. Although the reaction **4** → **5** via the **TS[45]** transition state (Figure 3) requires 29.2 kcal/mol (Table 3), the transition state itself is located 34 kcal/mol below the reactants. In the **TS[45]** structure the new C−Si and Si−H bonds of 1.826 and 1.594 Å, respectively, are nearly formed (cf. the relevant values in the product **5** of 1.748 and 1.476 Å). Following the IRC from **TS[45]** verifies that this transition state connects the *cis* form of the C−H insertion isomer $[H_2Si{-}CH{-}SiH]^+$ (**5**) with isomer **4**. Note that in view of the discussion in the previous paragraph, **TS[45]** may actually be the transition state that connects **3** with **5** since **4** may not exist.

The *trans* conformation of the C−H insertion isomer $[H_2Si{-}CH{-}SiH]^+$ (**6**) can be obtained from **5** in two ways. One way is a rotation of the SiH fragment through **TS[56r]**. The corresponding rotation barrier is about 11 kcal/mol relative to **5**, but the rotation transition state **TS[56r]** is still 46 kcal/mol below $Si^+ + SiH_2CH_2$. The second **5** → **6** interconversion mode, an inversion through **TS[56i]**, is, as expected, a more energy demanding process than the rotation. The computed inversion barrier is about 25 kcal/mol above **5**, but, as in the rotation case, the inversion transition state **TS[56i]** is lower in energy than the reactants by 32 kcal/mol. It is interesting to note here that all indicated bond angles in **5** and **6** are very close to 120°. The *cis* (**5**) and *trans* (**6**) forms of the $[H_2Si{-}CH{-}SiH]^+$ isomer are predicted to be very stable thermodynamically with respect to $Si^+ + SiH_2CH_2$, i.e., by 57−58 kcal/mol.

Starting from the thermodynamically very stable cyclic structure **3**, a H migration from Si to Si leading to another cyclic isomer, $[HSi{-}HSi{-}CH_2]^+$ (**12**), is possible. Structure **12** has two somewhat longer Si−C bonds than **3** and is thermodynamically much less stable, lying 25 kcal/mol above **3**. The energy required

to traverse the **3** → **12** transition state, denoted **TS[312]** (Figure 3), is 28 kcal/mol. However, **TS[312]** is nearly 40 kcal/mol below $Si^+ + SiH_2CH_2$, so this isomerization does not require an overall barrier. The structure of the 1,2-hydrogen migration transition state **TS[312]** reveals an almost completely formed Si−H bond of 1.557 Å.

The cyclic structure **3** is also the starting point for a 1,2-hydrogen shift from Si to C, resulting in the C_1 isomer $[HSi-Si-CH_3]^+$ (**7**). Structure **7** is essentially isoenergetic with **5** and **6**. Due to the appreciable spin contamination of the UHF wavefunction corresponding to **7** ($\langle S^2\rangle = 1.08$), its ROHF geometry is included for comparison (Figure 2). The largest difference between UHF and ROHF occurs for the Si−Si bond, which is 0.03 Å longer at ROHF as compared to UHF. The transition state **TS[37]** for the interconversion between **3** and **7** lies 35 kcal/mol above **3**. This is similar to the barrier for the 1,2-hydrogen shift from silaethylene to methylsilylene (*vide supra*). **TS[37]** is predicted to be 33 kcal/mol below the reactants, with partially broken Si−H and Si−C bonds of lengths 1.557 and 2.251 Å, respectively. Following the IRC from **TS[37]** on both the UHF and ROHF PES verifies that this transition state connects isomers **3** and **7**.

One can also reach the isomer $[HSi-Si-CH_3]^+$ (**7**) starting from $[Si\cdots HSi-CH_3]^+$ (**9**), via insertion of Si^+ into the (long and weak) Si−H bond. The corresponding transition state, **TS[79]**, is distorted from C_s symmetry with a C−Si−H−Si dihedral angle of about 120°. At the UHF/6-31G(d) level, **TS[79]** is only 0.5 kcal/mol above **9**. It drops to 0.5 kcal/mol *below* **9** at the ZPE-corrected PUMP4/6-31G(d,p) level of theory. Somewhat surprisingly, the ROHF counterpart of **TS[79]** connects complex **9** with a different isomer **8** (discussed below) rather than with **7**, as revealed by following the corresponding ROHF IRC. Consequently, the correct designation of this ROHF transition state is **TS[89]** (see Figure 5). An explanation for the dissimilarity of the two transition states is the appreciable spin contamination of **TS[79]** ($\langle S^2\rangle = 0.98$ vs 0.75 for the spin-corrected ROHF wavefunction).

A facile 1,2-hydrogen migration from the $[HSi-Si-CH_3]^+$ species (**7**) yields another methyl-containing $Si_2CH_4^+$ isomer, $[Si-SiH-CH_3]^+$ (**8**), mentioned above. For (C_s) **8**, the C−Si and Si−Si bonds of 1.865 and 2.353 Å, respectively, are close to the typical bond lengths for such single bonds, i.e., 1.89 and 2.34 Å, respectively. This isomerization product (**8**) is found to be the most thermodynamically stable isomer of $Si_2CH_4^+$, lying at 68.3 kcal/mol below $Si^+ + SiH_2CH_2$. However, the energy difference between **8** and **3** is only 0.4 kcal/mol (Table 2).

On the UHF surface, the **7** → **8** isomerization proceeds through the bridged intermediate **10**. This C_1 structure features a bridging hydrogen and a relatively short Si−Si distance of 2.225 Å; it also has noticeable spin contamination ($\langle S^2\rangle = 0.93$). The PUMP4 **7** → **10** transition state, **TS[710]**, is predicted to lie 62 kcal/mol lower in energy than the separated reactants. This is about 4 kcal/mol *below* isomer **7**, which therefore may not be a true minimum on the PES at higher levels of theory (or the MP4 transition state separating **7** and **10** is sufficiently shifted from the UHF structure that a small barrier may still exist).[4b] From the bridged species **10**, further migration of the bridging hydrogen occurs, leading to the lower-energy $[Si-SiH-CH_3]^+$ (**8**) isomer. This step involves transition state **TS[810]** with an associated barrier height of less than 1 kcal/mol relative to **10**.

It appears that the bridged structure **10** does not exist at the ROHF level, since **10** collapses to **8** upon ROHF geometry optimization. Therefore, the ROHF calculations suggest that the hydrogen migration from **7** to yield **8** proceeds directly via the transition state **TS[78]** (as verified by following the ROHF IRC, whose geometry is shown in Figure 5. However, at the higher and more reliable UQCISD level of theory, structure **10** is a local minimum on the PES; the resulting structure is also shown in Figure 2 for comparison. Including electron correlation results primarily in a large increase in the Si−Si−C bond angle, by nearly 30°. Moreover, the spin contamination in **10** essentially disappears, with $\langle S^2\rangle = 0.77$.

Finally, the insertion of Si^+ into a C−H bond of methylsilylene ($SiHCH_3$) starting from **13** yields $[HSi-CH_2-SiH]^+$ (**11**), about 36 kcal/mol below $Si^+ + SiH_2CH_2$. However, this insertion reaction must overcome an activation barrier that is 3.2 kcal/mol *above* $Si^+ + SiH_2CH_2$. Thus, similar to the insertion of Si^+ into a C−H bond of methylsilane,[4b] this particular insertion involves an overall barrier. The C−H insertion transition state, **TS[1113]**, has C_s symmetry (Figure 3), a partially formed C−Si bond of 2.33 Å, and a nearly fully formed Si−H bond of 1.537 Å. Walking down the minimum energy path from **TS[1113]** in one direction leads to the C−H insertion product $[HSi-CH_2-SiH]^+$ (**11**) and in the reverse direction to the methylsilylene complex **13**.

Conclusions

The following major conclusions emerge from the present *ab initio* study of the $Si_2CH_4^+$ potential energy surface (see the composite schematic of the potential energy surface in Figure 4).

(i) The formation of the $Si_2CH_4^+$ species reported here, including complex, Si−H, and C−H insertion products, and the other isomers of the $Si_2CH_4^+$ ion, is exothermic in all cases.

(ii) The transition states connecting the minima on the $Si_2CH_4^+$ potential surface are below the starting reactants; thus there appears to be no overall barriers involved in the processes considered. The two exceptions are (1) the 1,2-H migration TS connecting the initial complex $[Si\cdots H_2Si{=}CH_2]^+$ with its $SiHCH_3$ counterpart $[Si\cdots HSi-CH_3]^+$ and (2) the TS for insertion of Si^+ into a C−H bond of $SiHCH_3$, lying above the reactants $Si^+ + SiH_2CH_2$ by 1.0 and 3.2 kcal/mol, respectively.

(iii) The cyclic $[Si-H_2Si-CH_2]^+$ isomer **3** and the $[Si-SiH-CH_3]^+$ isomer **8** are predicted to be the most stable isomers of the $Si_2CH_4^+$ ion thermodynamically, with a ZPE-corrected PUMP4/6-31G(d,p) energy difference between **8** and **3** of only 0.4 kcal/mol. When the UCCSD(T)/6-31G(d,p) stabilities of the two isomers are examined (at the UHF/6-31G(d) geometries with ZPE corrections included), isomer **8** is again found to be more stable than **3** by 1.0 kcal/mol, whereas the bridged isomer **10** is 2.9 kcal/mol above **8** at this computational level.

(iv) There are a few noteworthy differences between the UHF and ROHF structures.

(v) Certain regions of the potential energy surface (e.g., **9** vs **TS**^{79}, **10** vs **TS**^{710}) are rather flat, so details of the PES may differ at higher levels of theory with larger basis sets.

Acknowledgment. This work was supported in part by grants from the National Science Foundation (CHE-9313717) and the Air Force Office of Scientific Research (F49620-95-1-0073). The calculations described here were performed on IBM RS6000 workstations generously provided by Iowa State University.

Supporting Information Available: Cartesian coordinates of the ROHF structures corresponding to the minima and transition states involved in the isomerization pathways considered in the paper (6 pages). Ordering information is given on any current masthead page.

OM9607309